Title: Central Himalayan rivers record the topographic signature of erosion by glacial lake outburst floods

Short title: The topography of glacial lake outburst floods

This manuscript has been submitted for publication in *Science Advances*. This version has not undergone peer review, and subsequent versions of this manuscript may have slightly different content. If accepted, the final version of this manuscript will be accessible via the 'Peer-reviewed Publication DOI' link on the right-hand side of this webpage. Please feel free to contact the authors, we welcome feedback.

Authors and Affiliations:

Maxwell P. Dahlquist[1, 2, 3*] and A. Joshua West[1, 4]

[1]*Department of Earth Sciences, University of Southern California, Los Angeles, California 90089, USA*

[2]*Department of Earth and Environmental Systems, Sewanee: The University of the South, Sewanee, Tennessee, 37383, USA*

[3]ORCID: 0000-0003-1445-6407

[4]ORCID: 0000-0001-6909-1471

*corresponding author: email - mpdahlqu@sewanee.edu

Abstract

In steep landscapes, river incision sets the pace of landscape evolution. Transport of coarse sediment controls incision by evacuating material delivered to river channels by landslides. However, large boulders that impede bedrock erosion are immobile even in major runoff-driven floods. Glacial lake outburst floods (GLOFs) mobilize these boulders and drive incision, yet their role in regional-scale erosion is poorly understood, largely because of their rarity. Here, we find a topographic signature of GLOF erosion in the Nepal Himalaya. In rivers with glaciated headwaters that generate GLOFs, valleys stay narrow and relatively free of sediment, with bedrock often exposed to erosion. In turn, tributaries to these valleys are steep so less efficient erosion mechanisms may keep pace with GLOF-driven incision. Where GLOFs are less frequent, valleys are more alluviated and incision stalls. Our results suggest the extent of headwater glaciation may play a central role in erosion of Himalayan river valleys.

Teaser

River valleys subject to glacial lake outburst floods have distinct patterns of channel slope and valley width compared to those without GLOFs.

Introduction

The erosion of mountainous topography crafts the shape of Earth's surface, influences atmospheric circulation and global climate, modulates global carbon and nutrient fluxes, and sets the tempo of natural hazards including earthquakes and landslides. At elevations above the equilibrium line altitude (ELA), snow persists from one year to the next, forming glaciers that carve textbook U-shaped valleys (*1*). Fierce debates have centered on the notion that a "glacial erosion buzz-saw" limits the total height and relief of mountain ranges (*2–5*), but even the proponents of this idea generally assume that the influence of glacial erosion fades below the ELA (*6*).

Many studies have noted the dramatic erosive power of GLOFs, which arise from the sudden and catastrophic draining of ice or moraine dammed lakes (*7–9*). The resulting floods can scour river valleys for 10s to 100s of kilometers downstream (*10–14*), in some cases mobilizing boulders that otherwise remain stationary even during heavy rainfall-driven flooding (*14*, *15*). The pace of the water bore from outburst floods exceeds that of entrained bedload, so the leading edge of the flood remains below its transport capacity and is capable of mobilizing material as it progresses downstream. These features make GLOFs highly effective incision mechanisms even in low-gradient channels (*14*, *16*). These events can thus extend the imprint of glacier-associated erosion well below the elevations that support glaciers themselves.

While the dramatic effects of GLOFs have been well-documented, their rarity has made it challenging to identify whether these floods are sufficiently frequent and widespread to play an important role in controlling the long-term evolution of mountain topography. Over-deepening downstream of glacially dammed valleys in the eastern Himalaya suggests that GLOF erosion may play more of a role than often recognized in the evolution of topography (*17*). Yet this effect is juxtaposed against the long-term inhibition of erosion as a result of lakes formed by glacial dams (*18*). Here, we evaluate the valley and channel morphology of rivers draining the Nepal Himalaya, revealing a systematic role for GLOFs as important agents of long-term erosion. Specifically, we compared rivers that have glaciated (or recently glaciated) headwaters versus those that do not, finding that rivers with glaciated headwaters are distinct both in valley width and channel steepness relationships between tributaries and trunk streams. Furthermore, we observe that knickpoints are concentrated in tributaries more likely to have experienced repeated GLOFs. We attribute these differences to the long-term imprint of repeated GLOFs. Our results suggest "top-down" glacially driven erosion may be important across more of the landscape in major mountain ranges than currently recognized, with fundamental implications for the coupling of tectonics, erosion, and landscape evolution, and for the interpretation of tectonic processes from river channel form.

The role of GLOF erosion in the Nepal Himalaya

The Nepal Himalaya are a leading exemplar of an actively eroding mountain range, offering unique opportunities for understanding the relationships between tectonics, topography, and erosion. The major rivers in Nepal have their headwaters in Tibet and flow across the High Himalaya and Middle Hills, ultimately draining onto the Gangetic Plain (Figure 1A). Tributaries to these rivers drain widely varying topography characterized by diverse geomorphic processes (*19*, *20*). Many of the major rivers have large areas of glaciated headwaters, and much attention has focused on the hazard posed by increasing GLOF frequency in a warming climate (*21*, *22*). Investigation of the role of GLOFs in shaping this landscape remains limited largely to individual case studies (*10*, *14*), along with identifying sedimentary evidence of past GLOF activity (*16*, *23*).

To test for a signature of pervasive GLOF control on erosion across the central Nepal Himalaya, we calculated metrics of river profile morphology, specifically **(1)** normalized channel steepness adjusted for precipitation and evapotranspiration, **(2)** the prevalence of knickpoints in tributary channels, and **(3)** valley width and normalized valley wideness. We interpreted the river channel metrics in the context of the upstream drainage area above the last glacial maximum

ELA (LGM ELA), estimated to have been 4200 meters in the Nepal Himalaya (*24*). We assume that the frequency of GLOFs was proportional to the potentially glaciated terrain in each basin.

We used the LGM ELA on the basis that river morphology expressed today reflects the integration of erosional processes over the several thousand years of glacial retreat (*25*). While outburst floods originating from landslide-dammed lakes are also common in the Himalaya and are also important geomorphic agents (*26*), we do not expect an obvious relationship between upstream glaciers and landslide-dammed lakes, so our analysis based on drainage area above the LGM ELA limits our focus to GLOF features. The assumption that drainage area above the ELA is proportional to GLOF frequency is imperfect, since, for example, the extent of glaciation on the Tibetan Plateau during the LGM is debated even though this area lies above the ELA (*27*). We account for this particular factor by excluding rivers that drain substantial area of the Tibetan Plateau from our analysis. We also reduce the likelihood of region-to-region variability in GLOF frequency affecting our results, by focusing our study area within the Central Himalaya region which is frequently considered as a coherent unit in hazard analyses of GLOFs (*28*, *29*). Fischer et al. (*29*) found that glacier mass balance (which is intrinsically tied to glacial volume) is related to the frequency of floods originating in moraine-dammed lakes. While the relationship between upstream drainage area above the ELA and outburst flood frequency is likely non-linear, we maintain that it is a reasonable proxy for regional-scale assessment.

Conceptual model for river morphologic response to GLOF erosion

At elevations below the extent of glaciation, rivers are the main pacemakers of erosion. The erosive power of rivers is controlled by their base level, which is the lowest elevation of active fluvial erosion. Uplift of mountainous terrain effectively decreases base level, driving rivers to steepen and incise more deeply into uplifting rock. This incision steepens surrounding hillslopes, which respond by eroding faster (*30*). Thus, fluvial erosion is driven "from the bottom up," whereby base level change begins at low elevations (e.g., at river outlets) and moves upstream from there, producing a wave of incision and hillslope lowering that works its way through the landscape (Figure 2A-C).

This simple conceptual model finds natural expression in fault-block mountains where uplift is focused on a single fault at the base of the range (*31*). In such settings and under the right conditions, the topographic profiles of rivers preserve quantitative information about the tectonic and geodynamic drivers of uplift, or about past change in climate (*19*). In more complex mountain ranges, numerous other processes can affect river incision and erosion, including differential rock uplift associated with multiple active tectonic features (*32*), gradients in precipitation and channel width (*33*, *34*), and variations in lithology and rock strength (*35*). In addition, extreme, infrequent events (such as GLOFs) have been shown to play key roles in erosion (*14*, *36*), yet their role in modulating the response of incision to uplift is poorly understood.

Morphometric proxies of GLOF erosion

We test for three predicted effects of GLOF-driven erosion on the topographic form of rivers in the central Himalaya. The first of these is the steepness of river channels. Normalized channel steepness (k_{sn}) represents the steepness of channels after accounting for the typically concave form of most river profiles. This concave form is reflected in a power law relationship between channel slope (S) and upstream area (A), where

$S = k_s A^{-\theta}$ (Eq. 1) (*37*).

If θ is fixed to a best-fit reference value, the normalized channel steepness k_{sn} provides a basis for comparing the relative steepness of different channels (see Methods). Differences in k_{sn}

between river segments have been attributed to variations in uplift (faster uplift requires a steeper, more energetic river for incision to keep pace), local rock strength (stronger rocks require more energy to erode), and climate (less discharge means less erosive power, requiring steeper channels). Importantly for our purposes, GLOFs may influence k_{sn} because they are highly effective erosional agents even in a low-gradient river. High-magnitude, low-frequency discharge events, of which lake outburst floods are the apotheosis, are recognized as a critical control on erosion and on the geometry of channels, particularly where discharge thresholds for initiation of erosion are high (*38–41*). Particularly, DiBiase and Whipple (*41*) proposed that erosional efficiency is enhanced under conditions where channel steepness is low, mean discharge and discharge variability are high, and incision thresholds are high. The major rivers of the Nepal Himalaya should meet these conditions, with discharge peaks defined by catastrophic outburst floods and incision thresholds governed by the presence of ~10 meter-scale boulders in the channel. We thus expect river segments that are influenced by GLOFs to erode more rapidly than rivers without GLOFs, all other factors being equal, and therefore GLOF-influenced rivers will require lower k_{sn} for the same erosion rate than if runoff-driven floods were the dominant erosional mechanism. If correct, this effect should be detectable in the geometry of the channels (Figure 2D).

Secondly and similarly, we expect GLOF erosion to be associated with discrete steepened reaches (knickpoints) in tributary channels near their outlets into larger trunk streams. In our proposed model for GLOF erosion, knickpoints should form in tributaries a result of pulses of GLOF incision in the trunk stream. A concentration of knickpoints near trunk streams where outburst floods are more frequent would support an erosion model where GLOFs are an important factor.

Thirdly, the removal of coarse sediment by GLOFs is expected to change river valley widths. We propose that outburst floods facilitate river incision by mobilizing very coarse sediment, including large boulders, that remains stationary even during large runoff-driven floods. The widths of valley floors should reflect the degree of aggradation at longer timescales than the width of the active channels (*42*, *43*). If floods clear out aggraded material, we expect to see a narrowing trend in rivers subject to more GLOF activity if our erosion model depicted in Figure 2D plays a substantial role of Himalayan river incision. To test this, we analyzed valley floor widths based on a discharge-adjusted normalized channel wideness index (k_{wn}^*, see Materials and Methods) to account for the typical power-law increase in valley width with discharge.

Results

Steepness ratios between tributaries and trunk streams

Along the course of the major Himalayan rivers, the mainstems typically drain glaciated areas, while many of the tributaries do not. We compared channel steepness between these by calculating the ratio of tributary k_{sn}^* (adjusted k_{sn} accounting for variability in discharge; see Materials and Methods) to trunk stream k_{sn}^* near where each tributary joins the mainstem (Figure 1B). Typically, unless a confluence coincides with the location of a lithologic contact, active deformation structure, or transient knickpoint, k_{sn}^* values in a mainstem and its tributary measured very close to the confluence should be approximately equal. We find that rivers with a greater proportion of upstream glaciated terrain have tributaries that are steeper near confluences (Figure 3A). We interpret this steepening of tributaries as being a response to accelerated incision rates in the trunk streams driven by GLOFs. Repeated GLOFs occurring from the same source areas along the same flow paths will produce a persistent difference in erosion rate between erosionally less efficient tributaries and GLOF-dominated trunk streams. This difference would require the tributaries that lack glaciated terrain to steepen to keep pace with erosion of the mainstem, increasing the k_{sn}^* ratio as we observe.

Knickpoint distribution and GLOF erosion

To verify whether patterns of knickpoints are consistent with GLOF incision being a prominent component of Himalayan erosion, we analyzed the distribution of knickpoints on tributaries within 2 kilometers of 4th or higher order rivers (Figure 1C). In 3062 tributary channels, we found 5970 knickpoints with at least 20 meters of relief. We log-binned knickpoint counts and total knickpoint relief by the amount of upstream drainage area above the ELA in the trunk stream that each tributary joins. We then assessed the proportion of knickpoints that are found in tributaries to rivers without glaciated headwaters, and we compared this proportion to that of tributary confluences in general. We found that knickpoints are much less common in tributaries to rivers with no glaciated drainage area upstream (Figure 4). Only ~18% of the knickpoints are found on tributaries to rivers without glaciated headwaters; in comparison, 30% of the tributaries analyzed drain to rivers with no drainage area above the ELA. This effect is more pronounced when knickpoints are weighted by relief, with only 15% of the total knickpoint relief found on these tributaries to unglaciated rivers. In tributaries to substantially glaciated rivers, we find over-representation of the knickpoints, an effect that is also accentuated when knickpoints are weighted by relief (Figure 4B).

The greater proportion of knickpoints and total knickpoint relief in the tributaries that drain into more glaciated channels support our conceptual model, wherein GLOF erosion creates knickpoints in tributaries at their confluences with the path of repeated outburst floods. These tributary knickpoints may stall at the confluences (*44*, *45*), or they may propagate upstream. By identifying knickpoints found up to 2 kilometers upstream from a potential GLOF path, we include both possibilities.

Interestingly, in both k_{sn}* ratios and knickpoint prevalence, we observe a threshold for the formation of these features. Around 10 km^2 of glaciated drainage area is required before the k_{sn}* ratios begin to increase (Figure 3). Similarly, knickpoint prevalence only increases where the trunk stream drains on the order of 10 km^2 of above-ELA terrain, although data are relatively scarce for lower areas (only 364 of 5970 knickpoints and 185 of 3062 tributary channels drain to trunk streams with between 1-10^7 m^2 of above-ELA terrain in their basins). Considering the apparent threshold in both metrics, we speculate that an upstream area of glaciated terrain on the order of 10 km^2 is required to produce recognizable outburst flood topography downstream in this region.

Valley widths and the role of GLOFs in "clearing the pipeline" of sediment

We expect that variation in valley floor width reflects the extent of alluviation. Wider valleys should have less frequent bedrock exposure, reflecting aggradation and slower incision. Valleys on GLOF paths should be systemically narrower than expected for a given discharge if GLOFs are clearing out sediment and driving rapid incision frequently enough to control river morphology. We measured the widths of valley floors and calculated a normalized wideness index, k_{wn}^*, adjusted for the expected power law increase in channel width with discharge incorporating the same discharge estimation as for k_{sn}^* (Allen et al., 2013; see Methods).

Measurements of valley width corroborate our inferences from k_{sn}^* and knickpoint occurrence: we find distinct trends in the relationship between valley width and discharge, with rivers that have upstream glaciers being narrower at lower discharges than rivers without glaciated headwaters (Figure 5A). Moreover, among rivers that do include glaciated terrain, valleys with more glaciated drainage area tend to have lower k_{wn}^* (Figure 5D). These observations suggest that GLOFs keep valley bottoms free of coarse sediment that broadens valleys and armors the bedrock channel bed against erosion. In other words, more frequent GLOFs "clear the pipeline", preventing clogging and allowing valleys to remain narrow. This is not simply a binary relationship, i.e., we do not see valleys with upstream glaciers relatively free of alluvium versus those without glaciers containing substantial fill, but rather find that the valley width appears to depend on the frequency or magnitude of the floods as inferred from upstream glaciated area (Figure 5D).

Discussion

The Physiographic Transition: Shift from "top down" to "bottom up" erosion

Altogether, our analysis suggests that rivers in the central Himalaya bear characteristic signatures of erosion by glacial outburst floods, suggesting that these events are an important but largely under-recognized mechanism of regional incision. Yet GLOFs can only be effective so far downstream. Cook et al. (*14*) studied two major GLOFs in the Bhote Khosi valley, occurring in 1981 and 2016, and identified the location of rollover points along the downstream river profile where GLOF discharges attenuated to the point that a monsoon flood with the same recurrence would have greater discharge. These points lie very near the prominent physiographic transition (PT) that separates the precipitous High Himalaya from the gentler Middle Hills to the south (Figure 1A).

The abruptness of the PT reflects the topographic response to a steep gradient in uplift rate and is associated with a pronounced increase in erosion rates from south to north (*30*, *46*).

Intriguingly, we find evidence for weakening of the influence of GLOFs on channel geometry when we look at tributary steepness relative to trunk streams above versus below the PT. The relationship between drainage area above the ELA and steepness ratio is no longer evident for confluences below the elevation of the 1981 GLOF rollover point (Figure 3B). These regions of the landscape that are only weakly affected by GLOF erosion would also explain why the highest above-ELA drainage area confluences have anomalously low k_{sn}^* ratios in Figure 3A. It thus appears that the PT may demarcate a shift in erosional process domain, representing the position above which "top-down" GLOF-driven incision is prominent enough to maintain a persistent topographic signature.

Implications for development of fluvial hanging valleys

"Fluvial hanging valleys" — steepened tributary reaches near their confluence with mainstem rivers — have been identified previously in the Himalaya and elsewhere. While often considered enigmatic features, their persistence in the landscape has been explained by erosional mechanics that produce lower erosional efficiency in steeper river reaches with low sediment flux (*44*, *45*). Not all of the steepened zones near confluences that we have identified represent true hanging valley geometry, but our analyses of both k_{sn}* ratios and knickpoint prevalence suggest that repeated outburst floods in a trunk stream may, under the correct conditions, control mainstem river incision and generate fluvial hanging valleys. In this case, we explain the formation of these features as resulting from the tributary steepening needed to keep pace with the GLOF-driven incision of the mainstem, producing persistent knickpoints near the location where tributaries enter trunk channels with upstream glaciation (Figures 2D-E). We thus propose a connection between the formation of fluvial hanging valleys and upstream glaciation that leads to GLOF-driven erosion in the mainstem.

Landscape evolution from the top down

A simple end-member model of fluvial incision involves the formation of a knickpoint, or localized steepening, in response to uplift which manifests as a drop in a river's base level (*19*) (Figures 2A-C). In this model, increased steepness causes localized increases in erosion, and the knickpoint propagates upstream. Complexity in this process of incision and knickpoint propagation has been increasingly recognized: channels dominated by bedload abrasion may have knickpoint retreat rates that are decoupled from overall incision rates (*47*, *48*), and knickpoints may be smoothed out over years to decades in the presence of copious bedload and sufficient discharge (*49*).

Our analysis of Himalayan river channels suggests that "top down" incision driven by GLOFs may be another important factor in driving erosion and determining channel morphology in glaciated mountain belts. Based on relationships we have documented between the area of glaciated headwaters, tributary channel steepness, knickpoint occurrence, and valley widths, we propose that incision processes in the High Himalayan rivers of central Nepal are influenced in important ways from above, by outburst floods from the headwaters of the trunk streams. A critical controlling factor for the geometry of tributaries is their steepening in response to GLOF erosion.

If this process is as pervasive elsewhere as our data suggest it is in the central Himalaya, it would have significant implications for the evolution of orogens in response to tectonic and climatic forcing. In particular, an important role for GLOF erosion, such as that we have identified, implies that the relationship between tectonics and erosion may be modulated by the migration of the ELA. If uplift pushes terrain above the ELA, it could create new glaciers and glacial lakes that, in turn, accelerate GLOF-driven incision. This feedback, in tandem with the propagation of knickpoints from below, could link uplift and erosion rates in ways not captured in current models of landscape evolution. Alongside the effect of tectonics, climatic shifts can drive the ELA to higher or lower elevations, shifting dominant process domains and their signature relief structures to higher or lower elevations. Studies of landscape evolution and interpretations of river channel morphology and network geometry in mountainous environments should consider the influence of outburst floods as regional drivers of erosion, even where glaciers are no longer present. Altogether, our results demand a rethinking of classic models of mountain river system evolution, to consider the role of glacial outburst floods as regional controls on erosion.

Materials and Methods

Physical Relationships in Channel Networks

In actively uplifting landscapes, the geometry of the land surface is governed by competition between uplift and gravity, mediated by a series of processes with a variety of controlling factors. In time, this competition tends to result in stalemate, a time-invariant condition of topographic steady state (*19*, *50*). For most of the Earth's surface, local boundary conditions for erosion are set by the pace of incision or aggradation associated with river channel processes. In channel networks, the relationship between channel slope and contributing drainage area can reveal the active erosional processes. Downstream reaches of the channel network, which are typically controlled by fluvial processes, are described by the power law function

$$E = KA^m S^n \quad \text{(Eq. 2)}$$

where E is erosion rate, K is the erosion coefficient, which is governed by local lithology, climate, and the process that control incision in the area, A is drainage area, S is local slope, and m and n are empirical constants which have a range of possible values depending on local conditions. Under steady-state conditions, where uplift and erosion can be assumed to be equal,

$$S = \left(\frac{U}{K}\right)^{\frac{1}{n}} A^{\frac{m}{n}} \text{ (Eq. 3)}$$

where U is uplift (*19*). This equation can be recast as Eq. 1, known as Flint's Law, where k_s defines a channel steepness $\left(\frac{U}{K}\right)^{\frac{1}{n}}$. The parameter θ = m/n, termed the concavity, represents the rate of change of channel slope with drainage area and is generally accepted to be insensitive to uplift rate (*37*). k_s varies with uplift rate but contains units that are dependent on θ. In order to make a reasonable comparison of k_s among channels with different θ, we must fix the value of θ to a reference concavity, θ_{ref}, that represents an average value for the channels in the area of interest, typically between 0.35-0.65, although this value may vary widely depending on local factors (*51*).

Adjusted normalized channel steepness index (k_{sn}*)

Fixing θ to θ_{ref} results in the normalized channel steepness index k_{sn} which is calculated as a best fit value for a given channel reach and is frequently and effectively used as a proxy in broad comparisons of uplift and incision rates across landscapes (*51*). However, a key feature of Eq. 1 is that drainage area A is used as a proxy for water discharge Q, which is the parameter presumed to drive incision. In general, larger drainage areas produce higher discharge, so that A can be assumed directly proportional to Q. However, given the dramatic gradient in precipitation from the Gangetic Plain to the Tibetan Plateau, contributing drainage area on its own is not an accurate proxy for discharge in this setting. We used a modified metric, k_{sn}^*, which accounts for variation in discharge across the region. To calculate k_{sn}^*, we estimated the contributing runoff from each DEM grid cell using mean annual precipitation (P) from a 12-year (1998-2009)

Tropical Rainfall Measuring Mission (TRMM) dataset (*52*) and evapotranspiration (ET) from the Global Land Evaporation Amsterdam Model (GLEAM) (*53*) and used the resulting runoff estimate to weight cells when calculating contributing drainage area. We recast Eq. 3 as

$S = k_{sn}^{*} Q^{-\theta_{ref}^{*}}$ (Eq. 4),

with Q representing estimated discharge from the water balance (P – ET) in each DEM cell. This approach ignores any spatial variation in water storage, which we expect to be small.

Employing our discharge estimate, we found a best-fit θ_{ref}^{*} of 0.0781 and used this value for all k_{sn}^{*} calculations in this study (Figure 3A). We used the Topographic Analysis Kit to calculate k_{sn}^{*} using the “trib” method, which fits k_{sn}^{*} for channel network segments between confluences individually, calculating tributaries separately from trunk streams for the most accurate representation of k_{sn}^{*} patterns near confluences (*54*). To compare tributary and trunk stream k_{sn}^{*}, we take the k_{sn}^{*} value for the tributary at the channel node closest to 200 meters from the confluence (Figure 1B). Given the resolution of the DEM (30 meter grid spacing) and possible orientations of channel nodes, this will be 5-7 nodes from the confluence. We use the k_{sn}^{*} value 200 meters from the confluence to avoid taking tributary k_{sn}^{*} values from stream segments that are in the valley bottom of the trunk stream. We set a minimum drainage area to define a stream as 0.48 km^2 following Roback et al. (*55*). In our k_{sn}^{*} ratio analysis, we have excluded confluences where the trunk valley at the confluence point has geometry that is indicative of erosion by direct glacial action (U-shaped valleys), confluences where the tributary channel was likely to have been glaciated in its headwaters at the LGM (and thus may have experienced GLOF erosion as well), and confluences where the trunk channel has extensive headwaters on the Tibetan Plateau. We excluded the last category because the extent of glaciation on the Tibetan Plateau is still debated and a wide range of possibilities may be realistic

(*27*). If regions above 4200 meters on the plateau were potentially ice-free at the LGM, then our proxy for GLOF frequency (total drainage area above the LGM ELA) does not apply in these rivers.

Eqs. 3 and 4 are derived from the detachment-limited stream power model (*56*), and a comparison of k_{sn}^* between channels assumes that both erode according to this model. Incision by lake outburst floods is a vastly more efficient process than incision by runoff-driven floods (*14*), in that it can do more erosive work on lower gradient channels with less contributing drainage area, meaning k_{sn} analysis could systematically underestimate incision in channels in which outburst flooding is an important geomorphic agent. Or, in very steep catchments such as those examined in this study, debris flows can control channel geometry at drainage areas of up to several square kilometers. Since channels incising due to debris flow action do not follow a power law relationship between slope and drainage area, the use of k_{sn}^* simply as an uplift-incision proxy in these catchments is problematic (*57*). We focus on k_{sn}^* in 1st and 2nd order basins where channel incision rate is controlled primarily by the frequency and runout of debris flows (*58*) as it relates to k_{sn}^* in the trunk channels, where, we argue, GLOF frequency is the primary factor controlling incision rate. This avoids direct comparison of k_{sn}^* in channels with different erosional mechanisms.

Knickpoint distribution

For our analysis of knickpoint distribution, we used the “knickpointfinder” function in TopoToolbox to identify and inventory knickpoints in the study area (*59*). Tributaries included in the knickpoint inventory are 1st or 2nd order streams that drain into 4th or higher order trunk streams and are at least 690 meters ASL. Similar to our k_{sn}* ratio analysis, we excluded tributaries to trunk streams that substantially drain the Tibetan Plateau since the extent of LGM glaciation on the plateau is much debated. We set a minimum relief of 20 meters as the threshold for inclusion, to minimize the possibility of false knickpoints arising from noise in the topographic data. Since knickpoints can arise from many different geologic processes, we conducted the knickpoint search on parts of the tributary network we assume to be most affected by potential geologically recent outburst floods in the trunk channel, within 2 kilometers of a trunk stream. The confluences included in Figure 4 are the confluences between tributaries included in the knickpoint search and trunk streams from which upstream drainage area above the ELA is reported.

Adjusted normalized channel wideness index (k_{wn}^*)

Most fluvial networks are characterized by a power-law increase in the width of channels as a function of contributing drainage area. This relationship is governed by many factors, including erosion rate, lithology, and climate, among others. Particularly in regions where extreme events can generate massive sediment inputs, channel width increases with aggradation (*42*) while relative channel width decreases with increased unit stream power, where bedrock is readily exposed and channels may incise downward (*60*). Dynamic channel width may thus be illustrative of channel response to tectonic or process-driven forcing. We can approach a width-area trend using an equation with the same form as slope-area, although the relationship between upstream drainage area and width is positive, so

$W = k_w A^b$ (Eq. 5),

where W is the channel width, k_w is a channel wideness index analogous to k_s. By fixing a best-fit reference value for b, we can examine local variation in channel wideness in response to enhanced erosion by increased GLOF activity.

To investigate the influence of GLOFs on channel width patterns, we used Google Earth imagery to make 1,598 width measurements from rivers across our study area, spacing measurements roughly equally along river reaches (Figures 2C, 5). We measured the widths of valley bottoms instead of the channels themselves, since the active channel can change in width rapidly with deposition from local landslides and subsequent evacuation of deposits. We determined the location of transitions from valley floors to hillslopes by observations of several features. Many valley bottoms have riparian vegetation that is visually distinct from vegetation on the hillslopes. In parts of the study area where valleys and hillslopes are developed for agriculture, farm terraces rapidly narrow where the hillslopes begin to steepen, offering a simple visual indication of the base of the hillslopes. Fluvial terraces are also visible in satellite imagery and aid in distinguishing active valley bottom from abandoned surfaces. We included terraces within ~10m of the elevation of the active channel in the valley bottom measurements, since a single outburst flood may incise enough to remobilize terrace material several meters above the active channel (*14*). Our assumption that the width of valley bottoms is analogous to the width of active channels is supported by the observed power law relationships between discharge and valley width in the field area (Figure 5A).

While the width of the active channel itself can vary significantly over a short time, we expect the width of the valley floor should reflect longer-term trends given that the timescales inherent in significantly raising or lowering an entire valley floor (and thus widening or narrowing it) should be orders of magnitude longer than timescales governing the width of the channel (*25*). As in our k_{sn}^* calculation, we use TRMM precipitation and GLEAM evapotranspiration data to estimate discharge, calculating a normalized channel wideness index as

$W = k_{wn}{}^{*} Q^{b_{ref}{}^{*}}$ (Eq. 6)

(*61*, *62*). Fits shown in Figure 5 were calculated using the "nlinfit" function in Matlab.

We used the Shuttle Radar Topography Mission (SRTM) 30-meter DEM for topographic analyses, patched with the Advanced Spaceborne Thermal Emission and Reflection Radiometer (ASTER) 30-meter DEM where voids exist in SRTM. All topographic metrics were calculated using the TopoToolbox and Topographic Analysis Kit packages for Matlab, and the DEM was preprocessed to remove outliers and impose a minimum downstream gradient for analysis of channel profiles (*54*, *59*).

Statistical analysis

Spearman rank correlation coefficients (Spearman's ρ) and p-values were calculated using the Matlab "corr" function with the "Spearman" parameter. Two-sample Kolmogorov-Smirnov tests were conducted and p-values calculated using the Matlab "kstest2" function.

Acknowledgments

General

We thank Kristen Cook, John Jansen, Jens Turowski, Georg Veh, and Missy Eppes for helpful discussions. We also thank William Medwedeff for the photograph used in Figure 2.

Funding

This work was supported by NSF award EAR-1640894.

Author Contributions

MPD and AJW conceived the study. MPD performed the analyses. MPD and AJW wrote the manuscript.

Competing Interests

The authors declare no competing interests.

Data and materials availability

Upon publication, the datasets generated and analyzed during the current study will be made available in the Hydroshare repository, http://www.hydroshare.org/resource/2883cfeebb3a43f2b9a1b222e2cfff29

References

1. Davis, William Morris, Glacial Erosion in France, Switzerland and Norway. *Proceedings of the Boston Society of Natural History*. **29**, 273–321 (1900).
2. N. Brozović, D. W. Burbank, A. J. Meigs, Climatic Limits on Landscape Development in the Northwestern Himalaya. *Science*. **276**, 571 (1997).
3. D. L. Egholm, S. B. Nielsen, V. K. Pedersen, J.-E. Lesemann, Glacial effects limiting mountain height. *Nature*. **460**, 884–887 (2009).
4. S. N. Thomson, M. T. Brandon, J. H. Tomkin, P. W. Reiners, C. Vásquez, N. J. Wilson, Glaciation as a destructive and constructive control on mountain building. *Nature*. **467**, 313–317 (2010).
5. M. T. Cunningham, C. P. Stark, M. R. Kaplan, J. M. Schaefer, Glacial limitation of tropical mountain height. *Earth Surface Dynamics*. **7**, 147–169 (2019).
6. G. Prasicek, F. Herman, J. Robl, J. Braun, Glacial Steady State Topography Controlled by the Coupled Influence of Tectonics and Climate. *Journal of Geophysical Research: Earth Surface*. **123**, 1344–1362 (2018).
7. Mason, Kenneth, Indus floods and Shyok glaciers. *The Himalayan Journal*. **1**, 10–29 (1929).
8. Haeberli, Wilfried, Frequency and Characteristics of Glacier Floods in the Swiss Alps. *Annals of Glaciology*. **4**, 85–90 (1983).
9. D. R. Montgomery, B. Hallet, L. Yuping, N. Finnegan, A. Anders, A. Gillespie, H. M. Greenberg, Evidence for Holocene megafloods down the tsangpo River gorge, Southeastern Tibet. *Quaternary Research*. **62**, 201–207 (2004).
10. D. A. Cenderelli, E. E. Wohl, Flow hydraulics and geomorphic effects of glacial-lake outburst floods in the Mount Everest region, Nepal. *Earth Surface Processes and Landforms*. **28**, 385–407 (2003).

11. E. R. C. Baynes, M. Attal, S. Niedermann, L. A. Kirstein, A. J. Dugmore, M. Naylor, Erosion during extreme flood events dominates Holocene canyon evolution in northeast Iceland. *Proceedings of the National Academy of Sciences*. **112**, 2355–2360 (2015).

12. J. Jacquet, S. W. McCoy, D. McGrath, D. A. Nimick, M. Fahey, J. O'kuinghttons, B. A. Friesen, J. Leidich, Hydrologic and geomorphic changes resulting from episodic glacial lake outburst floods: Rio Colonia, Patagonia, Chile. *Geophysical Research Letters*. **44**, 854–864 (2017).

13. K. A. Lang, K. W. Huntington, D. R. Montgomery, Erosion of the Tsangpo Gorge by megafloods, Eastern Himalaya. *Geology*. **41**, 1003–1006 (2013).

14. K. L. Cook, C. Andermann, F. Gimbert, B. R. Adhikari, N. Hovius, Glacial lake outburst floods as drivers of fluvial erosion in the Himalaya, 6 (2018).

15. D. Xu, Characteristics of debris flow caused by outburst of glacial lake in Boqu river, Xizang, China, 1981. *GeoJournal*. **17** (1988), doi:10.1007/BF00209443.

16. J. L. Pickering, M. S. Diamond, S. L. Goodbred, C. Grall, J. M. Martin, L. Palamenghi, C. Paola, T. Schwenk, R. S. Sincavage, V. Spieß, Impact of glacial-lake paleofloods on valley development since glacial termination II: A conundrum of hydrology and scale for the lowstand Brahmaputra-Jamuna paleovalley system. *GSA Bulletin*. **131**, 58–70 (2019).

17. D. Scherler, H. Munack, J. Mey, P. Eugster, H. Wittmann, A. T. Codilean, P. Kubik, M. R. Strecker, Ice dams, outburst floods, and glacial incision at the western margin of the Tibetan Plateau: A >100 k.y. chronology from the Shyok Valley, Karakoram. *Geological Society of America Bulletin*. **126**, 738–758 (2014).

18. O. Korup, D. R. Montgomery, K. Hewitt, Glacier and landslide feedbacks to topographic relief in the Himalayan syntaxes. *Proceedings of the National Academy of Sciences*. **107**, 5317–5322 (2010).

19. K. X. Whipple, G. E. Tucker, Dynamics of the stream-power river incision model: Implications for height limits of mountain ranges, landscape response timescales, and research needs. *Journal of Geophysical Research: Solid Earth*. **104**, 17661–17674 (1999).

20. D. R. Montgomery, E. Foufoula-Georgiou, Channel network source representation using digital elevation models. *Water Resources Research*. **29**, 3925–3934 (1993).

21. O. Korup, F. Tweed, Ice, moraine, and landslide dams in mountainous terrain. *Quaternary Science Reviews*. **26**, 3406–3422 (2007).

22. G. Veh, O. Korup, A. Walz, Hazard from Himalayan glacier lake outburst floods. *Proceedings of the National Academy of Sciences*. **117**, 907–912 (2020).

23. M. L. Huber, M. Lupker, S. F. Gallen, M. Christl, A. P. Gajurel, "Timing of exotic, far-travelled boulder emplacement and paleo-outburst flooding in the central Himalaya"

(preprint, Physical: Geomorphology (including all aspects of fluvial, coastal, aeolian, hillslope and glacial geomorphology), 2020), , doi:10.5194/esurf-2020-17.

24. K. Asahi, Equilibrium-line altitudes of the present and Last Glacial Maximum in the eastern Nepal Himalayas and their implications for SW monsoon climate. *Quaternary International*. **212**, 26–34 (2010).

25. Y. Ray, P. Srivastava, Widespread aggradation in the mountainous catchment of the Alaknanda–Ganga River System: timescales and implications to Hinterland–foreland relationships. *Quaternary Science Reviews*. **29**, 2238–2260 (2010).

26. K. Hewitt, Catastrophic landslides and their effects on the Upper Indus streams, Karakoram Himalaya, northern Pakistan. *Geomorphology*. **26**, 47–80 (1998).

27. N. Kirchner, R. Greve, A. P. Stroeven, J. Heyman, Paleoglaciological reconstructions for the Tibetan Plateau during the last glacial cycle: evaluating numerical ice sheet simulations driven by GCM-ensembles. *Quaternary Science Reviews*. **30**, 248–267 (2011).

28. G. Veh, O. Korup, S. von Specht, S. Roessner, A. Walz, Unchanged frequency of moraine-dammed glacial lake outburst floods in the Himalaya. *Nature Climate Change*. **9**, 379–383 (2019).

29. M. Fischer, O. Korup, G. Veh, A. Walz, “Controls of outbursts of moraine-dammed lakes in the greaterHimalayan region” (preprint, Glaciers/Natural Hazards, 2020), , doi:10.5194/tc-2020-327.

30. D. W. Burbank, A. E. Blythe, J. Putkonen, B. Pratt-Sitaula, E. Gabet, M. Oskin, A. Barros, T. P. Ojha, Decoupling of erosion and precipitation in the Himalayas. *Nature*. **426**, 652–655 (2003).

31. A. C. Whittaker, How do landscapes record tectonics and climate? *Lithosphere*. **4**, 160–164 (2012).

32. E. Kirby, K. Whipple, Quantifying differential rock-uplift rates via stream profile analysis. *Geology*. **29**, 415 (2001).

33. G. H. Roe, D. R. Montgomery, B. Hallet, Orographic precipitation and the relief of mountain ranges: OROGRAPHIC PRECIPITATION AND RELIEF. *Journal of Geophysical Research: Solid Earth*. **108** (2003), doi:10.1029/2001JB001521.

34. N. J. Finnegan, G. Roe, D. R. Montgomery, B. Hallet, Controls on the channel width of rivers: Implications for modeling fluvial incision of bedrock. *Geology*. **33**, 229 (2005).

35. L. S. Sklar, W. E. Dietrich, Sediment and rock strength controls on river incision into bedrock. *Geology*. **29**, 1087 (2001).

36. J. W. Kirchner, R. C. Finkel, C. S. Riebe, D. E. Granger, J. L. Clayton, J. G. King, W. F. Megahan, Mountain erosion over 10 yr, 10 k.y., and 10 m.y. time scales. *Geology*. **29**, 591 (2001).

37. J. J. Flint, Stream gradient as a function of order, magnitude, and discharge. *Water Resources Research*. **10**, 969–973 (1974).

38. N. P. Snyder, K. X. Whipple, G. E. Tucker, D. J. Merritts, Importance of a stochastic distribution of floods and erosion thresholds in the bedrock river incision problem: FLOODS AND THRESHOLDS IN RIVER INCISION. *Journal of Geophysical Research: Solid Earth*. **108** (2003), doi:10.1029/2001JB001655.

39. D. Lague, N. Hovius, P. Davy, *Journal of Geophysical Research: Earth Surface*, in press, doi:10.1029/2004JF000259.

40. J. M. Turowski, E. M. Yager, A. Badoux, D. Rickenmann, P. Molnar, The impact of exceptional events on erosion, bedload transport and channel stability in a step-pool channel. *Earth Surface Processes and Landforms*. **34**, 1661–1673 (2009).

41. R. A. DiBiase, K. X. Whipple, The influence of erosion thresholds and runoff variability on the relationships among topography, climate, and erosion rate. *Journal of Geophysical Research*. **116** (2011), doi:10.1029/2011JF002095.

42. W. Schwanghart, A. Bernhardt, A. Stolle, P. Hoelzmann, B. R. Adhikari, C. Andermann, S. Tofelde, S. Merchel, G. Rugel, M. Fort, O. Korup, Repeated catastrophic valley infill following medieval earthquakes in the Nepal Himalaya. *Science*. **351**, 147–150 (2016).

43. B. J. Yanites, N. A. Mitchell, J. C. Bregy, G. A. Carlson, K. Cataldo, M. Holahan, G. H. Johnston, A. Nelson, J. Valenza, M. Wanker, Landslides control the spatial and temporal variation of channel width in southern Taiwan: Implications for landscape evolution and cascading hazards in steep, tectonically active landscapes: Variation in channel morphology controlled by landslides in s. Taiwan. *Earth Surface Processes and Landforms*. **43**, 1782–1797 (2018).

44. B. T. Crosby, K. X. Whipple, N. M. Gasparini, C. W. Wobus, Formation of fluvial hanging valleys: Theory and simulation. *Journal of Geophysical Research*. **112** (2007), doi:10.1029/2006JF000566.

45. J. K. Goode, D. W. Burbank, Numerical study of degradation of fluvial hanging valleys due to climate change. *Journal of Geophysical Research*. **114** (2009), doi:10.1029/2007JF000965.

46. C. W. Wobus, K. X. Whipple, K. V. Hodges, *Tectonics*, in press, doi:10.1029/2005TC001935.

47. J. D. Jansen, D. Fabel, P. Bishop, S. Xu, C. Schnabel, A. T. Codilean, Does decreasing paraglacial sediment supply slow knickpoint retreat? *Geology*. **39**, 543–546 (2011).

48. A. Wilson, N. Hovius, J. M. Turowski, Upstream-facing convex surfaces: Bedrock bedforms produced by fluvial bedload abrasion. *Geomorphology*. **180–181**, 187–204 (2013).

49. K. L. Cook, J. M. Turowski, N. Hovius, A demonstration of the importance of bedload transport for fluvial bedrock erosion and knickpoint propagation: BEDLOAD TRANSPORT AND FLUVIAL INCISION. *Earth Surface Processes and Landforms*. **38**, 683–695 (2013).

50. S. D. Willett, M. T. Brandon, On steady states in mountain belts. *Geology*. **30**, 175 (2002).

51. C. Wobus, K. X. Whipple, E. Kirby, N. Snyder, J. Johnson, K. Spyropolou, B. Crosby, D. Sheehan, in *Special Paper 398: Tectonics, Climate, and Landscape Evolution* (Geological Society of America, 2006; https://pubs.geoscienceworld.org/books/book/569/chapter/3802975/), vol. 398, pp. 55–74.

52. B. Bookhagen, High Resolution Spatiotemporal Distribution of Rainfall Seasonality and Extreme Events Based on a 12-year TRMM Time Series (2013).

53. B. Martens, D. G. Miralles, H. Lievens, R. van der Schalie, R. A. M. de Jeu, D. Fernández-Prieto, H. E. Beck, W. A. Dorigo, N. E. C. Verhoest, GLEAM v3: satellite-based land evaporation and root-zone soil moisture. *Geoscientific Model Development*. **10**, 1903–1925 (2017).

54. A. M. Forte, K. X. Whipple, Short communication: The Topographic Analysis Kit (TAK) for TopoToolbox. *Earth Surface Dynamics*. **7**, 87–95 (2019).

55. K. Roback, M. K. Clark, A. J. West, D. Zekkos, G. Li, S. F. Gallen, D. Chamlagain, J. W. Godt, The size, distribution, and mobility of landslides caused by the 2015 M w 7.8 Gorkha earthquake, Nepal. *Geomorphology*. **301**, 121–138 (2018).

56. A. D. Howard, A detachment-limited model of drainage basin evolution. *Water Resources Research*. **30**, 2261–2285 (1994).

57. J. D. Stock, W. E. Dietrich, Erosion of steepland valleys by debris flows. *Geological Society of America Bulletin*. **118**, 1125–1148 (2006).

58. M. P. Dahlquist, A. J. West, Initiation and Runout of Post-Seismic Debris Flows: Insights From the 2015 Gorkha Earthquake. *Geophysical Research Letters*. **46**, 9658–9668 (2019).

59. W. Schwanghart, D. Scherler, Short Communication: TopoToolbox 2 – MATLAB-based software for topographic analysis and modeling in Earth surface sciences. *Earth Surface Dynamics*. **2**, 1–7 (2014).

60. T. Croissant, D. Lague, P. Steer, P. Davy, Rapid post-seismic landslide evacuation boosted by dynamic river width. *Nature Geoscience*. **10**, 680–684 (2017).

61. G. H. Allen, J. B. Barnes, T. M. Pavelsky, E. Kirby, Lithologic and tectonic controls on bedrock channel form at the northwest Himalayan front: BEDROCK CHANNEL FORM,

MOHAND, INDIA. *Journal of Geophysical Research: Earth Surface*. **118**, 1806–1825 (2013).

62. B. J. Yanites, The Dynamics of Channel Slope, Width, and Sediment in Actively Eroding Bedrock River Systems. *Journal of Geophysical Research: Earth Surface*. **123**, 1504–1527 (2018).

Figures and captions

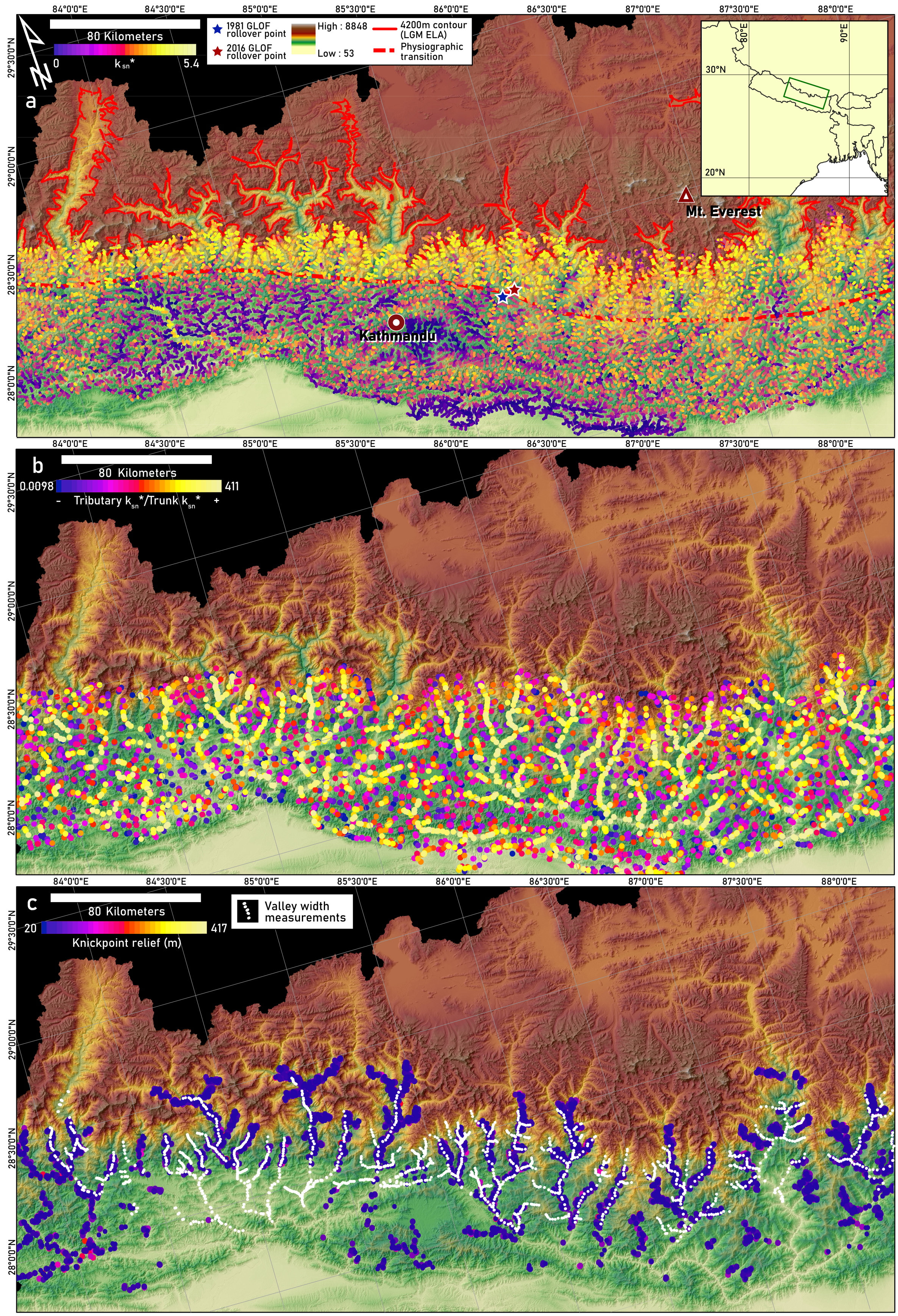

84°0'0"E
84°30'0"E
85°0'0"E
85°30'0"E
86°0'0"E
86°30'0"E
87°0'0"E
87°30'0"E
88°0'0"E
29°30'0"N
29°0'0"N
28°30'0"N
28°0'0"N
80 Kilometers
0
k_{sn}*
5.4
a
1981 GLOF rollover point
2016 GLOF rollover point
High : 8848
Low : 53
4200m contour (LGM ELA)
Physiographic transition
80°E
90°E
30°N
20°N
Mt. Everest
Kathmandu
b
80 Kilometers
0.0098
411
- Tributary k_{sn}*/Trunk k_{sn}* +
c
80 Kilometers
Valley width measurements
20
417
Knickpoint relief (m)

Fig. 1. Maps of study area showing geomorphic indices and other points of interest

1A. Overview map of the study area, showing equilibrium line altitude at the Last Glacial Maximum (LGM ELA) along with other points of interest. k_{sn}^* values are overlain on river network for elevations below LGM ELA and were calculated only where direct glacial action did not appear to be a major erosion mechanism. **1B.** k_{sn}^* ratios at confluences included in this study, where Strahler order 1 and 2 tributaries enter order 3 or higher trunk streams. Markers are placed at the confluence where the k_{sn}^* ratio was measured. **1C.** Locations and relief of knickpoints included in analyses, and locations of valley width measurements.

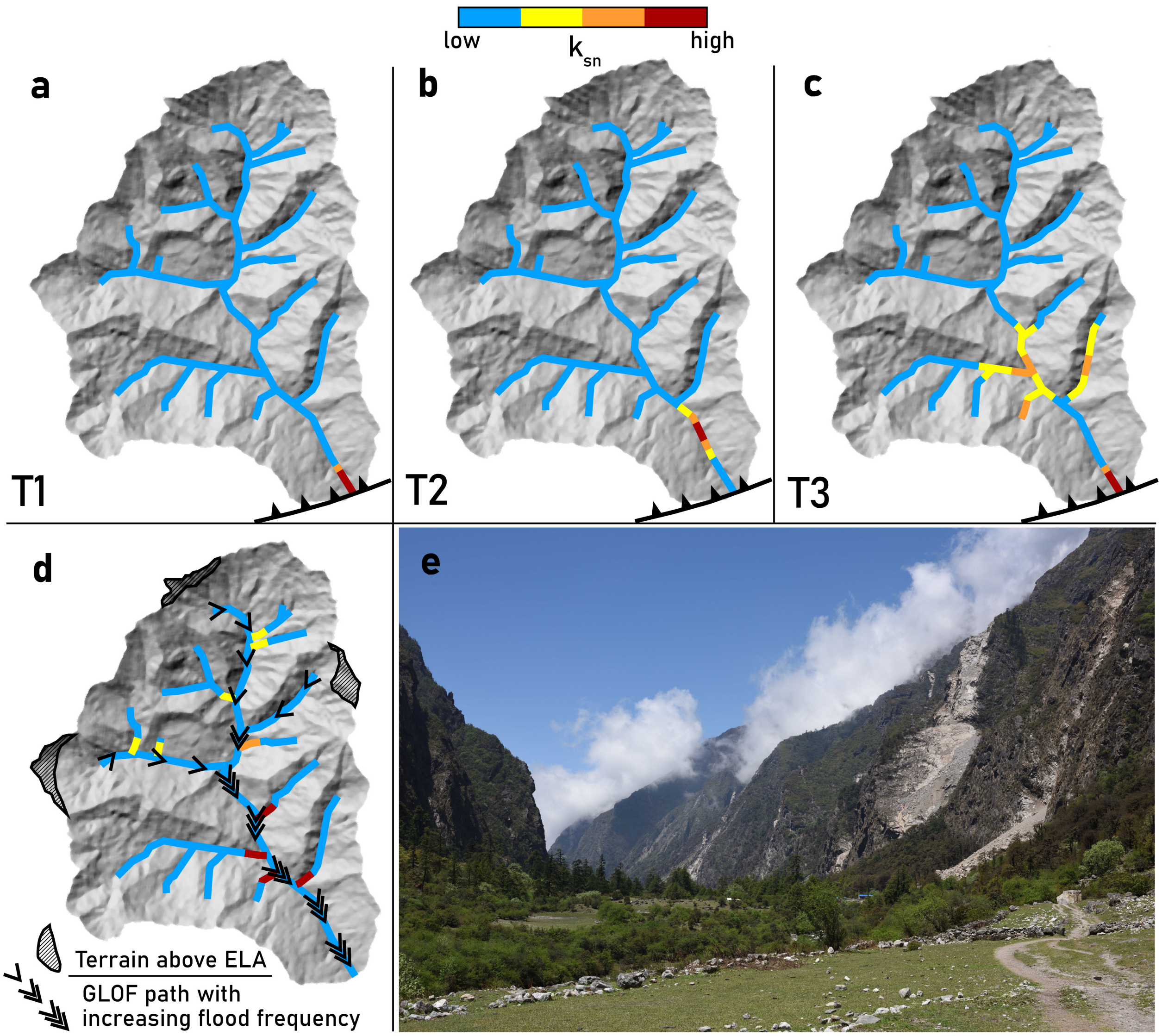

Fig. 2. Conceptual models of erosion with and without GLOFs.

2A-2C. Schematic of predicted k_{sn} patterns arising from erosion driven by upstream knickpoint migration resulting from base level fall, including knickpoint diffusion described in alluvial and bedrock-alluvial channels (Rosenbloom and Anderson, 1994). 1A-1C represent time steps showing the evolution of k_{sn} patterns following a base level fall initiating at the thrust fault at the outlet of the catchment (T1 to T3 reflects temporal progression). In 1C, a second base level fall has initiated. **2D.** Schematic of steady state k_{sn} patterns we hypothesize to arise from erosion driven by GLOFs originating from the high-elevation regions shown as terrain above ELA. Our aim in illustrating the simple scenario shown in panels A-C is not to suggest it as a plausible representation of the tectonic geomorphology of the Himalaya, but instead to contrast the end-member expectations from erosion purely driven by changes in base level versus the conceptual model we propose for glacial lake outburst flood (GLOF)-driven erosion, in panel D — while recognizing that actual erosion in Himalayan river valleys will involve an collaboration between these end-member scenarios. **2E.** Photograph from Langtang Valley, Nepal, showing steep inner valley walls and steep tributary catchments entering the trunk valley ~1 kilometer below the lowest identified glacial surfaces. Photo location is 28.200° N, 85.460° E.

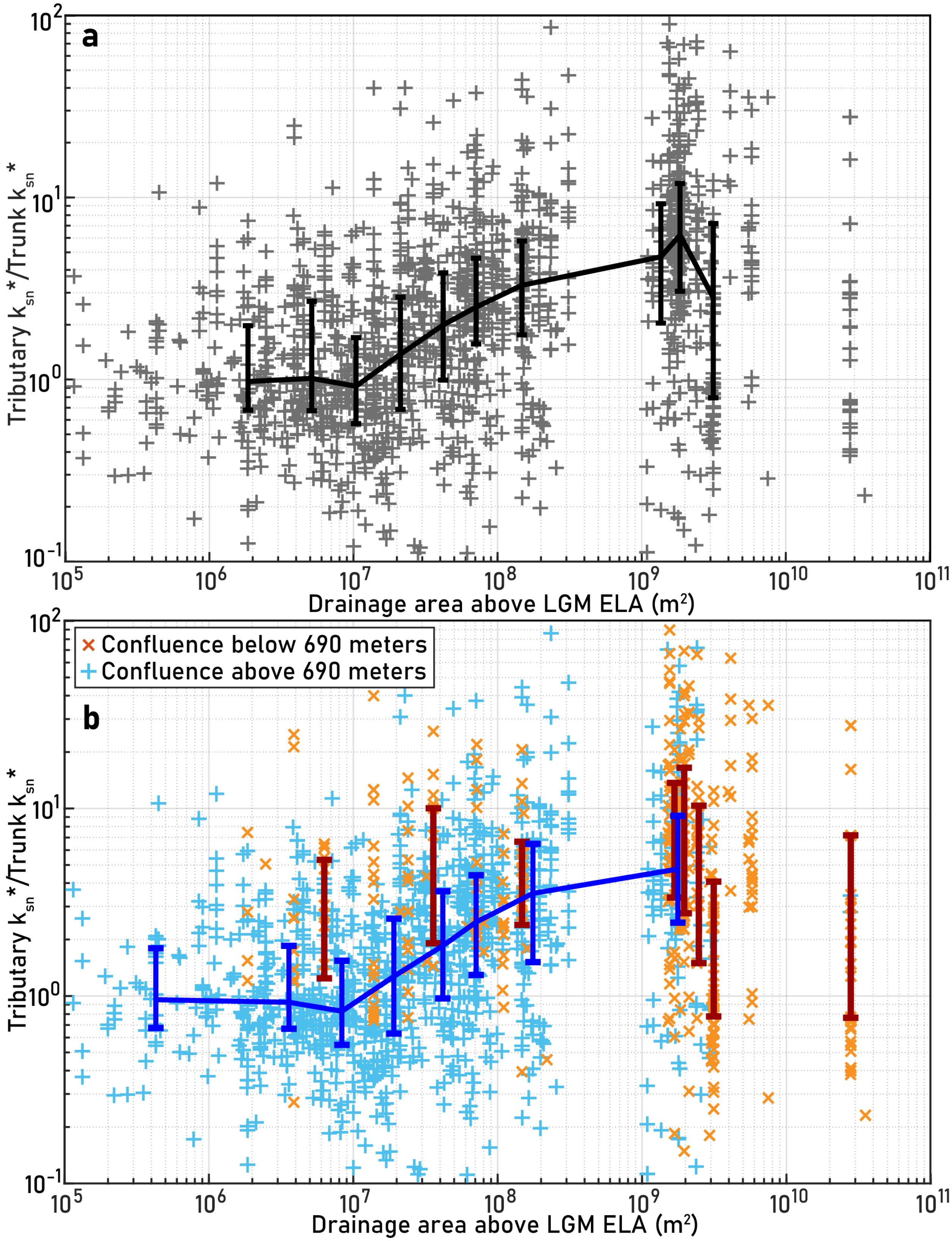

Fig. 3. Adjusted normalized steepness index ratios between tributaries and trunk streams

vs. glaciated drainage area in the trunk stream

3A. k_{sn}^* ratios between tributaries and trunk streams measured at confluences versus upstream area above the LGM ELA in the trunk stream. Bin centers are median values, edges are upper and lower quartiles. **3B.** k_{sn}^* ratios at confluences separated into those above and below 690 meters, the elevation of the 1981 Bhote Koshi outburst flood discharge rollover point. We use 690 meters as an approximate elevation of the PT in major river channels, to test for the influence of GLOF erosion on valley geometry above vs. below the PT. Spearman's rank correlation coefficient (Spearman's ρ), which tests for a potentially nonlinear monotonic relationship, for data above 690 meters is $\rho = 0.441$ with $p < 0.01$. We also conducted a two-sample Kolmogorov-Smirnov test for the distributions of k_{sn}^* ratios with above-ELA drainage areas between 10^7-10^8 m^2 ($n = 488$) and 10^9-10^{10} m^2 ($n = 155$) to determine if the samples come from significantly different distributions, and found the empirical CDF for the first group is larger with $p < 0.01$.

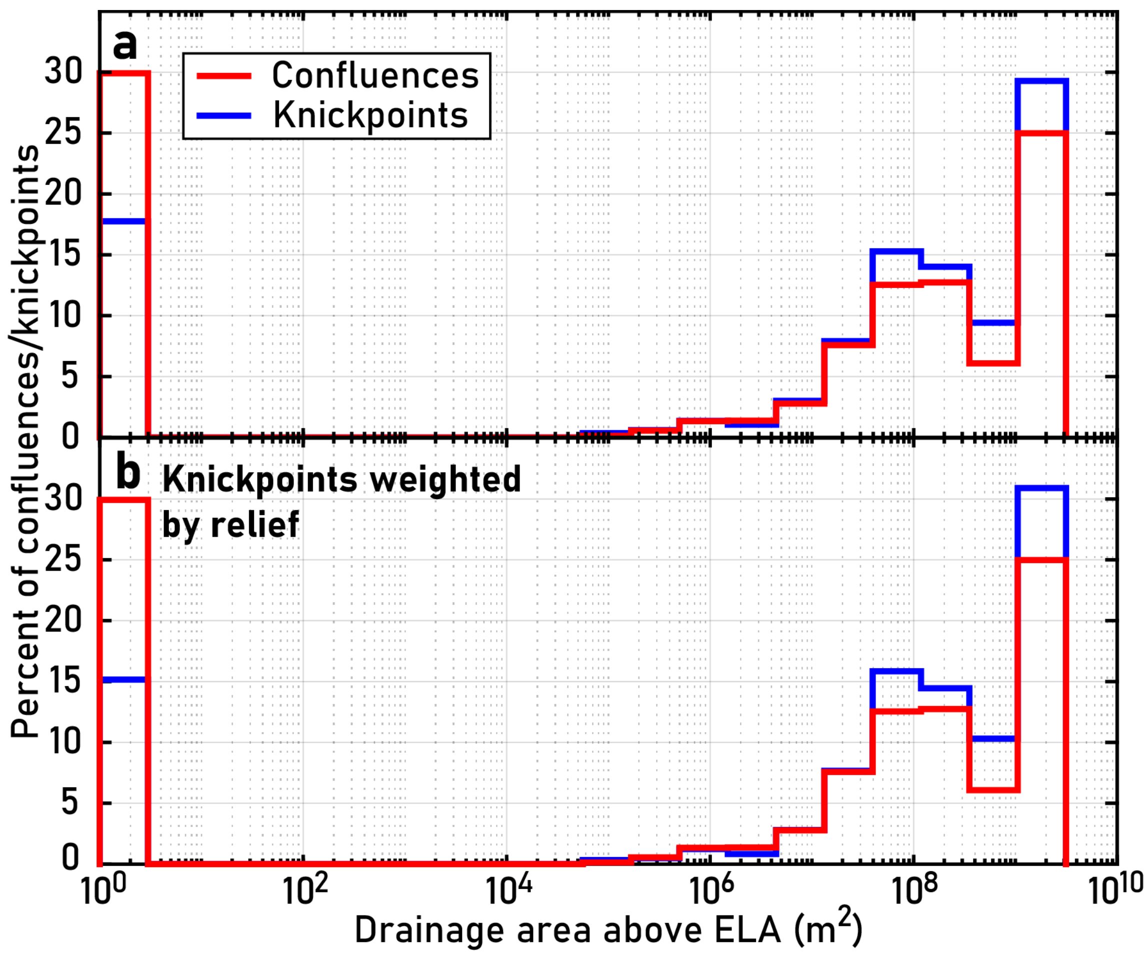

Fig. 4. Distributions of knickpoints and channel confluences with respect to glaciated drainage area in the trunk stream

4A. Distribution of knickpoints (n = 5970) and confluences (n = 3062) between 1st and 2nd and 4th or higher order rivers with respect to the area of terrain above the ELA drained by the trunk stream. Knickpoints included in the analysis are located on a 1st or 2nd order tributary within 2 km of a confluence with a 4th or higher order trunk stream. Area is log-binned, the lowest area bin contains only knickpoints and confluences where the trunk stream does not drain any terrain above the ELA. See Methods for criteria for identifying knickpoints. **4B.** Same as 4A, but knickpoints are weighted by their relief. For both the relief-weighted and non-weighted knickpoint distributions, we conducted two-sample Kolmogorov-Smirnov tests for the distributions of knickpoints versus confluences with respect to above-ELA drainage areas and found the empirical CDF for the confluences is larger with $p < 0.01$.

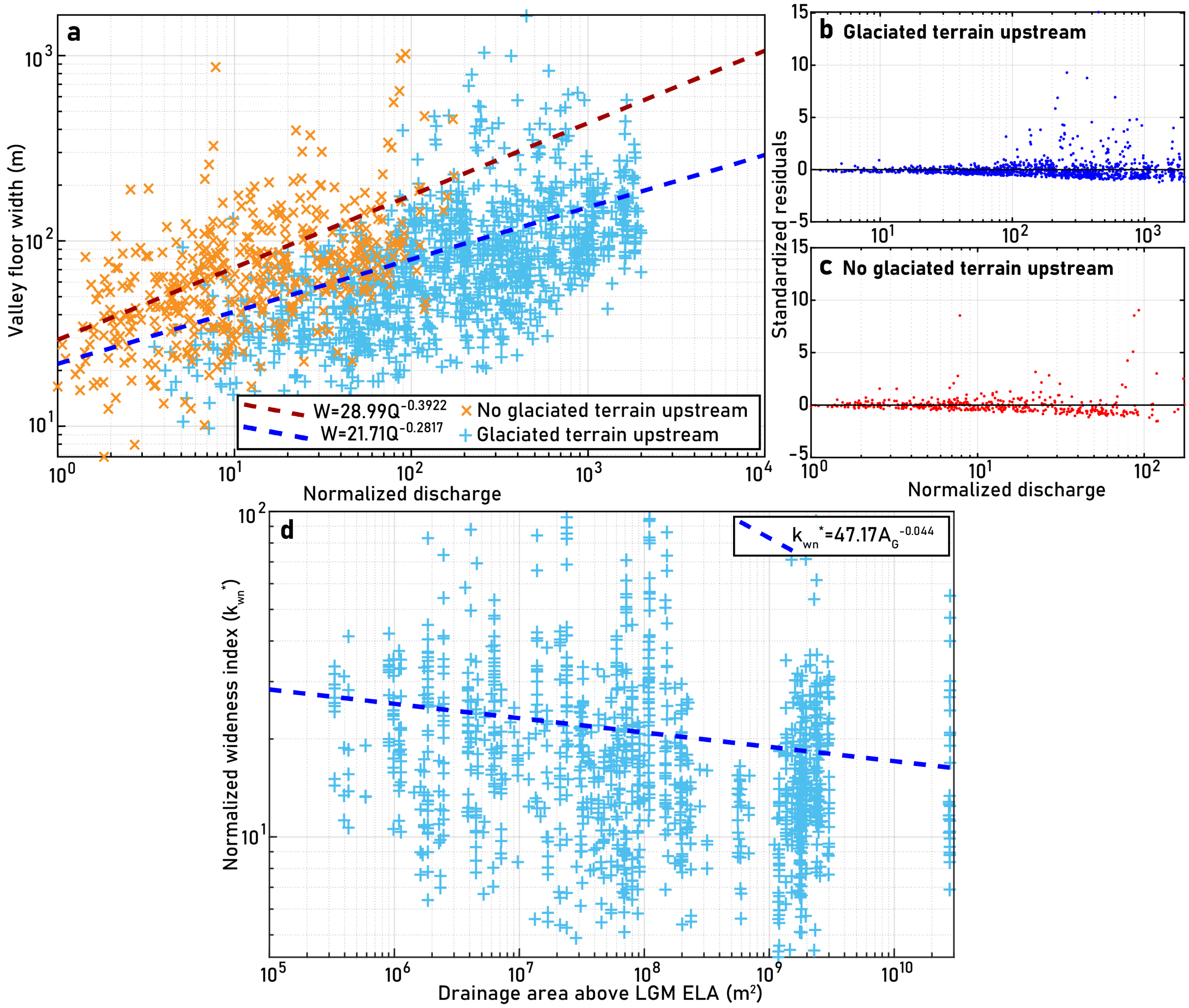

Fig. 5. Channel width versus discharge and adjusted normalized wideness index versus glaciated drainage area in the trunk stream

5A. Valley floor width versus discharge for rivers with and without headwaters above the LGM ELA, with power-law fits for valley wideness. Locations of valley width measurements are shown in Figure 2C. **5B & 5C.** Residuals plots for power-law fits shown in Figure 5A. **5D.** Normalized wideness (k_{wn}^*) versus contributing drainage area above the LGM ELA for valley width measurements in blue from Figure 5A, using the power law fit in 3C. Here, A_G refers to drainage area above the ELA. Spearman's $\rho = -0.2116$ with $p < 0.01$. We conducted a two-sample Kolmogorov-Smirnov test for the distributions of k_{wn}^* ratios with above-ELA drainage areas between 10^7-10^8 m^2 ($n = 332$) and 10^9-10^{10} m^2 ($n=378$) and found the empirical CDF for the latter group is larger with $p < 0.01$.